(Received 1 February 2024, Accepted 5 April 2024, Scheduled 14 April 2024)

A 1-Bit Metasurface with Adjustable Focus Achieved by Rotating Array

Bo Yin[1], Shubin Wang[1,*], Yun Li[2], and Hao Zhang[1]

[1]*School of Optoelectronic Engineering, Chongqing University of Posts and Telecommunications, Chongqing, China*
[2]*China Coal Technology & Engineering Group Chongqing Research Institute Co., Ltd, Chongqing, China*

ABSTRACT: The application scenarios of near-field focusing metasurfaces usually require scanning the target area. Passive metasurface requires a turntable to complete scanning due to its limited functionality. The active metasurface typically has a high cost because it needs to load PIN diodes. To address this issue, the article introduces a 1-bit reconfigurable metasurface that can achieve multi-focus tunability under fixed polarization through a rotating array. The 1-bit polarization-independent metasurface unit consists of three layers of metal. The top layer of the unit consists of three rectangular patches in the X-direction; the middle layer is a cross-shaped patch structure; and the bottom layer is a metal ground. The cross-shaped structure in the middle layer can easily provide the 1-bit reflection phase required for two orthogonal polarizations independently. Using a vertically polarized horn to illuminate the metasurface, the top layer's X-direction rectangular patches do not provide phase for vertical polarization. By rotating the array where the cross-shaped patches are located by 90°, the phase shift provided can achieve two focal points. On this basis, rotate the upper array by 90°, making the rectangular patches change from the X-direction to the Y-direction. Meanwhile, the current of the cross-shaped patches is blocked under vertical polarization illumination. By changing the upper rectangular patches, a third independent phase can be provided. After size optimization, a third focus can be formed. The proposed 1-bit focusing-adjustable metasurface array has a simple structure, low cost, and enhanced utilization rate of the metasurface array. It has a high application prospect in projects such as microwave imaging.

1. INTRODUCTION

Near-field focusing can converge electromagnetic waves from the transmitting source at a certain point in near-field region within the outer boundary of $2D^2/\lambda$ [1]. Near-field focusing technology was originally applied to wireless power transmission [2, 3]. Additionally, this technology has a wide range of application scenarios, such as millimeter wave imaging [4], biomedicine [5], and radio frequency identification [6]. Since the concept of near-field focusing was proposed in the 1960s, it has been achieved in various ways. Traditional methods have drawbacks, such as the difficulty of processing parabolic reflector [7], the complexity of microstrip phased array feed [8], and the low efficiency of Fresnel zone plates [9]. As an emerging technology in the past decade, metasurfaces have excellent phase control capabilities, providing a new path for near-field focusing [10].

On the other hand, wireless energy transmission requires changing the focusing position, and microwave imaging requires the antenna to complete scanning of the target area. The application scenarios of near-field focusing require metasurfaces to meet more diverse and flexible practical requirements. Improving the focusing effect is a problem that needs to be solved. In general, active metasurfaces can provide more phase combinations to generate more focal points. The functionality of the array can be changed by utilizing the change in phase of the individual elements with frequency. In 2021, Zhao et al. [11] and in 2022 Tao et al. [12] proposed a W-band frequency-varying polarization metasurface for imaging applications. The feeding module is a disordered-cavity, which can generate different internal field distributions at different working frequencies. The frequency-diverse feature of the field distribution would be inherited by the coupling slots and passed on to the radiation patterns of the frequency-polarization-diverse metasurface antenna. The phase-random-modulation metasurface contains a variety of different metamaterial elements with different transmission phases and diverse polarization characteristics, which could generate polarization-diverse radiation patterns when being excited by electromagnetic waves with different polarizations. This unit can achieve scanning of the target area with the focus varying with the frequency of the feed source. However, it must be noted that designing units with frequency-agile characteristics is challenging (in the paper, one element consists of 16 sub-units), and to achieve more functions requires occupying a wider frequency band. When PIN diodes, varactor diodes, or other components are integrated into the metasurface and loaded with control circuitry, programmable metasurfaces can be obtained. Ratni et al. designed a reconfigurable one-dimensional metasurface by installing varactor diodes on the unit cells, which can focus the incident plane wave in the near-field region under certain conditions [13]. In 2020, Han et al. proposed a 1-bit encoding unit tuned by PIN diodes operating at 35 GHz, which generates randomly complex beams to sample the target area and achieves near-field imaging [14]. Similarly, Li et al. proposed a 2-bit reconfig-

* Corresponding author: Shubin Wang (1411768919@qq.com).

urable metasurface unit operating in the C band. The PIN diodes loaded in the unit can change the reflection phase of the unit to achieve near-field dynamic focusing [15]. These metasurfaces loaded with diodes have very high costs and complex power supply circuits. Mei et al. utilized polarization independence to achieve a 2-bit dual-channel metasurface [16]. Zhang et al. utilized a dual-polarization metasurface with independent regulation characteristics to achieve multiple focusing functions such as single feed source with single focus and single feed source with dual focal points [17]. By adjusting the size of each nanobrick and using different orientation angles, Li et al. can control the amplitude and phase to achieve a dual channel metasurface [18]. A double-layered C-shape reflective meta-atom is designed by Li et al. to realize independent phase control with high efficiency. This unit has been used to achieve a dual channel metasurface [19]. In Liu et al.'s research, the propagation phase is combined with the geometric phase to generate diverse phase delays, enabling the metasurface to be multiplexed under two nonorthogonal polarization states to achieve four-channel image displays [20]. The method of realizing multiple focus points using passive metasurfaces is usually achieved through polarization independence. However, each polarization provides a phase for the array, which limits the number of functionalities of the array. Here, the proposed metasurface with adjustable triple foci under the same polarization greatly expands the functionality of the metasurface.

This article proposes a 1-bit metasurface that achieves adjustable focusing by rotating the array. The metasurface unit consists of three layers of metal. The middle layer of the unit has a cross-shaped patch with polarization-independent tuning characteristics. Under Y-polarized incident waves, the lower layer array can be rotated to achieve two independent focusing characteristics. At the same time, the upper layer X-direction rectangular patch does not affect the working state of the array for y polarization. Finally, after rotating the upper metasurface array by 90°, the upper layer unit becomes a Y-direction rectangular patch. In this state, the upper layer unit and middle layer unit constitute a new Y-polarization phase, achieving a third focus. The simulated electric field results also verify the effectiveness of the designed array.

2. THE METHOD & ANALYSIS OF ADJUSTABLE FOCUS

This section describes the scheme of generating multiple focal points related to polarization by using metasurface. Figure 1 illustrates the schematic diagram of the proposed scheme, which consists of a feed source and a metasurface. The strategy for generating adjustable multi-focus beams is to rotate the upper and lower layers of the metasurface by 90° under the condition of fixed source polarization. This requires the metasurface to provide independent phases in horizontal and vertical polarizations to generate tunable multi-focus beams.

According to the theory of electromagnetic wave propagation, phase is equal to the product of wave number and wave path. The distance between each unit on the reflecting metasurface and the target focal point position is $|\overrightarrow{r_d} - \overrightarrow{r_{ij}}|$. It may be assumed that the reflecting metasurface is a phase reference

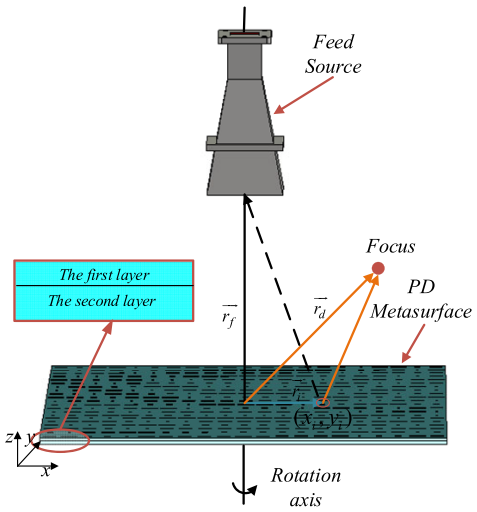

FIGURE 1. The proposed adjustable focus metasurface schematic.

surface. Then, for the focal point, the phase distribution required to produce the focal point belongs to the wave behind the reference surface, so the phase distribution required to produce the focal point in space can be obtained as Eq. (1).

$$\varphi_d(x_i, y_i) = \arg\left(\exp\left(-jk_0\left|\overrightarrow{r_d} - \overrightarrow{r_{ij}}\right|\right)\right) = -k_0\left|\overrightarrow{r_d} - \overrightarrow{r_{ij}}\right| \quad (1)$$

Figures 2(a), (b), (c) take a 21×21 array as an example (with a unit period of p), and shows the possible phase distribution for generating three foci with different positions. Since the realization of the adjustable focus function requires phase states with different states, it is necessary to perform 1-bit discrete processing on the above phases, that is:

$$\varphi(x_i, y_i) = \begin{cases} 0 & -90° \le \varphi_d(x_i, y_i) < 90° \\ 180° & -180° \le \varphi_d(x_i, y_i) < -90°, \\ & 90° \le \varphi_d(x_i, y_i) < 180° \end{cases} \quad (2)$$

The 1-bit phase obtained by discretizing the phases in Figures 2(a), (b), (c) is shown in Figures 2(d), (e), (f). To realize the adjustable three-focus function, a fixed Y-polarized feed source is used to illuminate the array. First, the lower layer independently provides phase state 1 to achieve focusing at POSITION 1. Then, the lower layer array is rotated by 90° to change the phase of the Y-polarization to achieve focusing at

TABLE 1. Phase shift combinations required to achieve the tunable PD metasurface with three points.

FOCUS POSITION 1	FOCUS POSITION 2	FOCUS POSITION 3
−90°	−90°	−90°
−90°	−90°	90°
−90°	90°	−90°
−90°	90°	90°
90°	−90°	−90°
90°	−90°	90°
90°	90°	−90°
90°	90°	90°

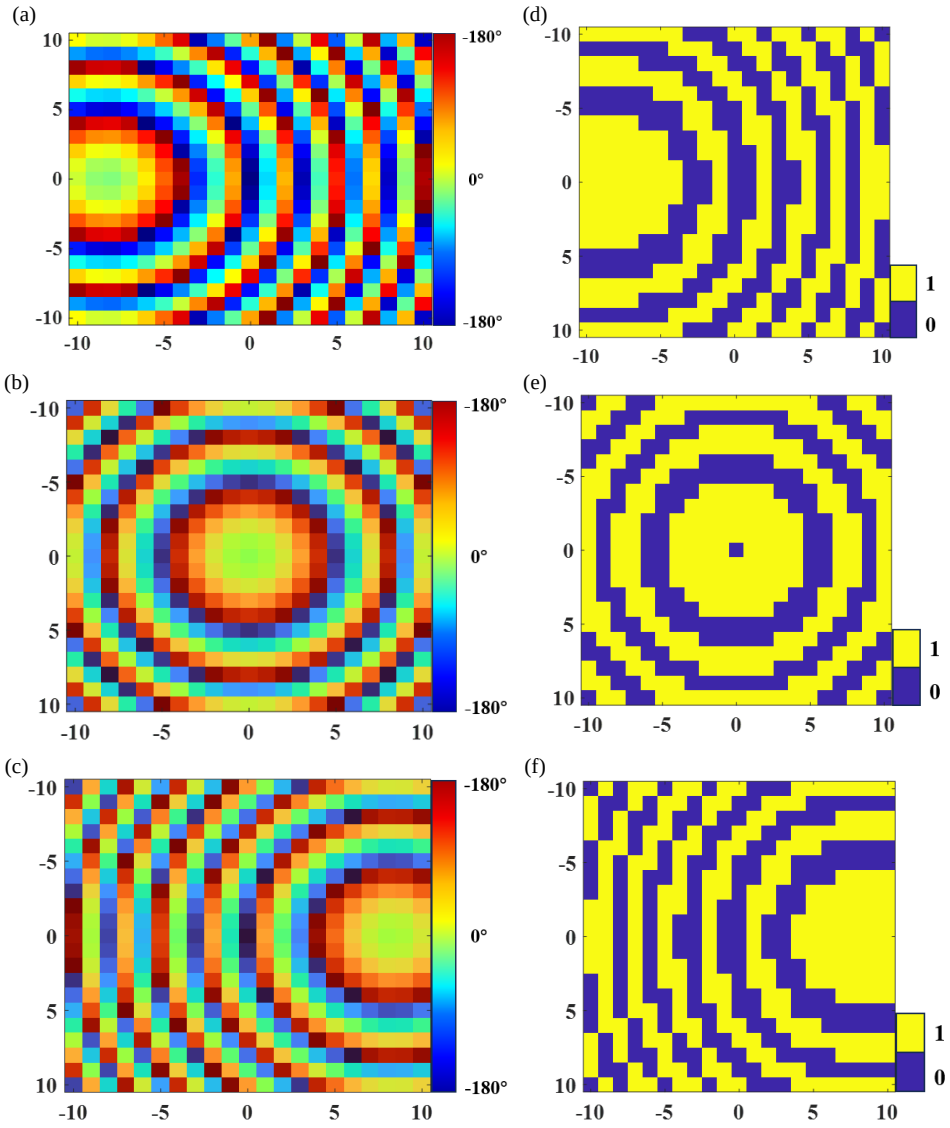

FIGURE 2. Phase distribution. (a) POSITION 1 $(-125, 0, 250)$; (b) POSITION 2 (0, 0, 250); (c) POSITION 3 (125, 0, 250); (e) discrete phase $(-125, 0, 250)$; (e) discrete phase (0, 0, 250); (f) discrete phase (125, 0, 250).

POSITION 2 with phase state 2. Finally, the upper layer array is rotated by 90°, and the upper and lower layers jointly provide phase to achieve focusing at POSITION 3 with phase state 3.

According to the phase distribution in Figure 2, the phase required for each focus can be obtained. It is found that 8 sets of phase shift combinations are needed to realize the required phase difference (PD) metasurface, as shown in Table 1.

3. ELEMENT DESIGN AND ARRAY SIMULATION

The designed structure of the metasurface is shown in Figure 3. The metasurface is a three-layer structure, consisting of an upper X-direction rectangular patch, a middle cross-shaped metal patch, and a lower metal ground plane. The dielectric substrate is made of F4B ($\varepsilon_r = 2.2$), with an upper layer of 2 mm thickness and a lower layer of 3 mm thickness. It is worth noting that in order to allow independent rotation of the upper and lower layers, the two layers of dielectric substrates are not bonded together.

The simulation results of the surface current of the designed metasurface element are shown in Figure 4 by CST Microwave Studio software. It can be seen from the figure that when the incident wave is polarized in the Y-direction and l_2 placed horizontally, the current intensity of l_2 and l_3 is much smaller than that of l_1. Meanwhile, the phase is mainly controlled by changing the length of l_1. When l_3 is rotated by 90°, the current direction of l_3 is opposite to that of l_1. Since l_3 is above l_1, the surface current density of l_3 is stronger than that of l_1. At this time, the phase of the unit can be controlled by changing the length of l_1.

As shown in Figure 5, when l_3 is placed horizontally, the reflection amplitude of the metasurface unit at 10 GHz is greater than 0.95. By changing the length of l_1, the reflection phase range reaches approximately 180°, satisfying the 1-bit phase

Phase shift combination	l_1	l_2	l_3
$-90^\circ \sim -90^\circ \sim -90^\circ$	8.1 mm	8.1 mm	5 mm
$-90^\circ \sim -90^\circ \sim 90^\circ$	8.1 mm	8.1 mm	13.1 mm
$-90^\circ \sim 90^\circ \sim -90^\circ$	8.1 mm	11 mm	5 mm
$-90^\circ \sim 90^\circ \sim 90^\circ$	8.1 mm	11 mm	13.1 mm
$90^\circ \sim -90^\circ \sim -90^\circ$	11 mm	8.1 mm	10.3 mm
$90^\circ \sim -90^\circ \sim 90^\circ$	11 mm	8.1 mm	2 mm
$90^\circ \sim 90^\circ \sim -90^\circ$	11 mm	11 mm	10.3 mm
$90^\circ \sim 90^\circ \sim 90^\circ$	11 mm	11 mm	2 mm

TABLE 2. Reflection phase corresponding to different sizes.

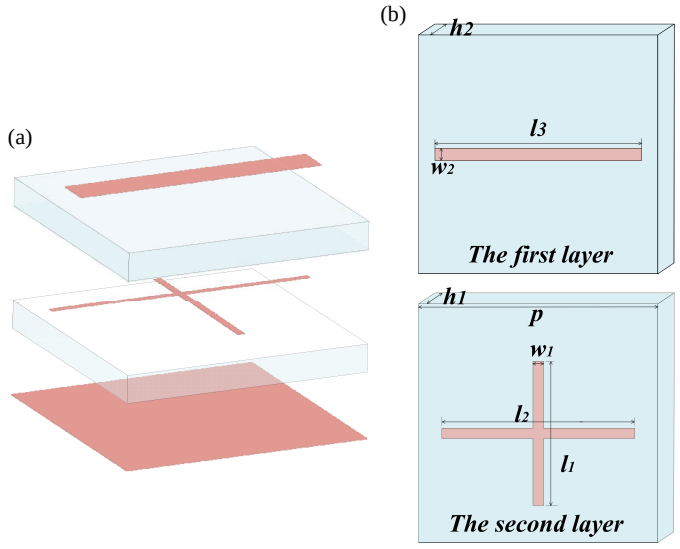

FIGURE 3. Schematic of the designed metasurface unit structure, (a) side view; (b) top view.

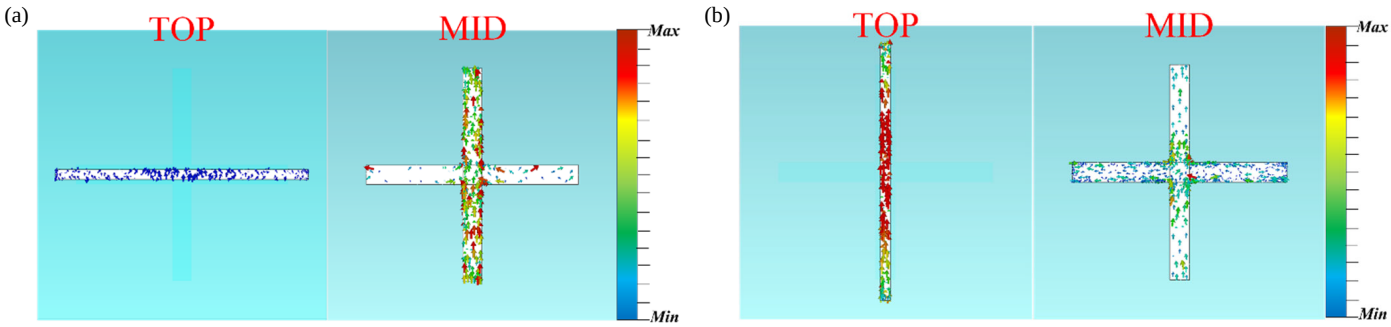

FIGURE 4. The surface current of the element, (a) before rotation; (b) after rotation.

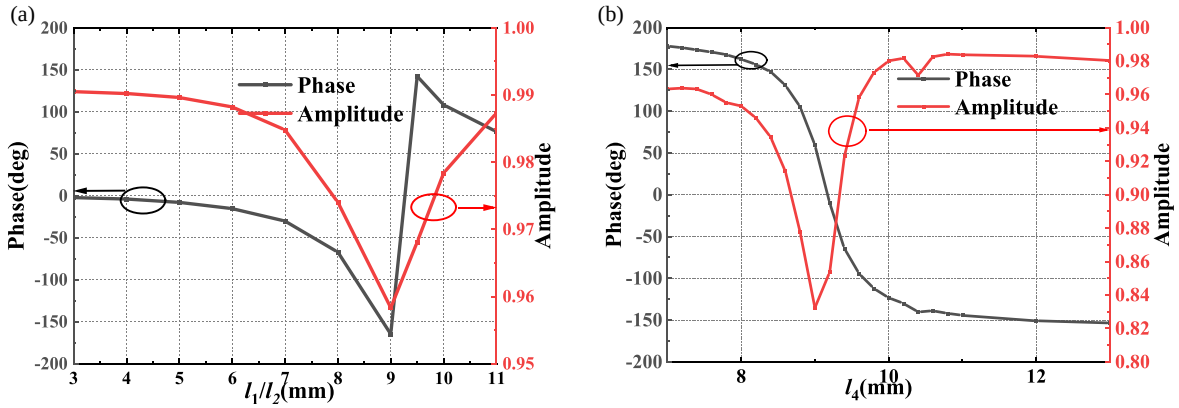

FIGURE 5. The reflection amplitude and phase curve of the metasurface, (a) l_3 is horizontal; (b) l_3 is vertical.

amplitude, which indicates that rotating the lower cross pattern can produce two focal points. Similarly, after rotating l_3 by 90°, the reflection amplitude of the metasurface unit is also greater than 0.95. By changing the length of l_3, the reflection phase range reaches 180°, satisfying the 1-bit phase amplitude and meeting the design requirement for achieving the third focus.

To meet the phase requirements of the array, the elements are digitized by 1-bit. Adjusting the sizes of l_1, l_2, l_3 can provide different reflection phases, and the sizes of l_1, l_2, l_3 are summarized in Table 2. It can be seen from Table 2 that the phase and critical dimension corresponding relationship of the elements in POSITION 1 and POSITION 2 are the same. The main de-

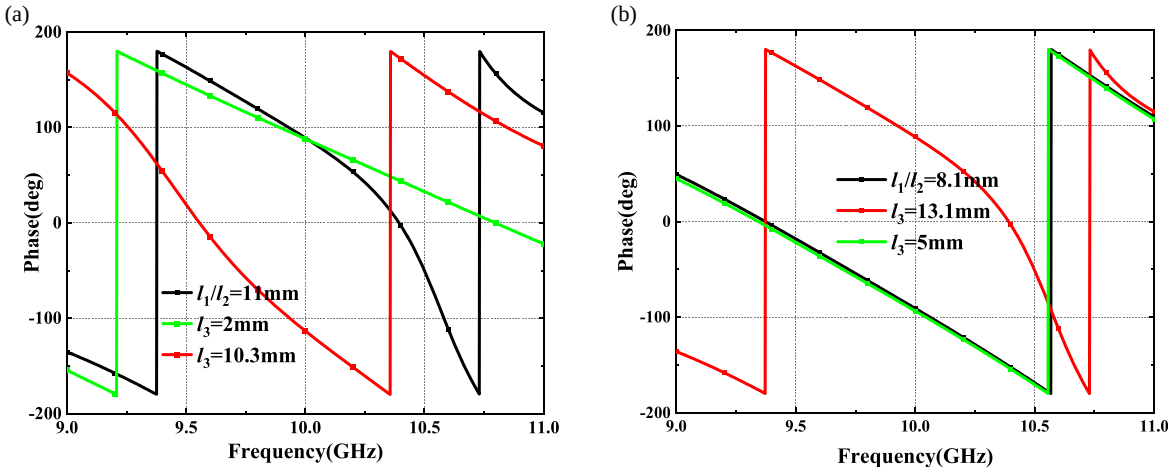

FIGURE 6. Phase characteristics.

sign difficulty of the element lies in the phase of POSITION 3, which is composed of l_1 and l_3. After determining the lengths of l_1 and l_2 to achieve the first two phases, different lengths of l_1 and l_3 need to form the same phase, mainly by changing l_3 to achieve the phase of POSITION 3. The corresponding relationship between these reflection phases and element lengths is shown in Figure 6.

According to the phase distributions shown in Figures 2(d), (e), and (f), as well as the relationship between the sizes in Table 2 and the reflection phases, the PD element surface is realized. Figure 7 gives the respective patterns of the metasurfaces that produce different focal positions. The simulation results show that POSITION 1 and POSITION 2 can achieve normal focusing. However, when realizing the focusing of POSITION 3, the focal point of POSITION 1 also exists. The focusing effect of POSITION 1 is better than that of POSITION 3. This is due to the second layer cross-shaped currents. As can be seen from Figure 2, when l_3 is working, the currents on l_1/l_2 cannot be ignored, and they will continue to focus at POSITION 1. It is necessary to further improve the unit to reduce the intensity of the second layer currents when l_3 is working.

4. DESIGN IMPROVEMENT

The improved unit structure and its current distribution are shown in Figure 8. The width w_2 of the lengthened rectangular patch l_3 is increased to be greater than the width w_1 of the second-layer cross-shaped patch. When l_3 is working, it will completely block the lower layer l_1, which can reduce the current intensity of the lower layer patches. To ensure that l_3 can completely block lower layer l_1, the length of l_3 needs to be greater than the maximum value of l_1 and less than the period P of the unit. However, l_3 cannot ensure the 180° phase width required for 1-bit metasurfaces within this range. Therefore, two symmetric rectangular patches ($l_4 = l_5$) are added on both sides of l_3. By setting the length of l_3 to be greater than the maximum value of l_1/l_2, the third independent phase is adjusted by changing the length of l_4/l_5.

To meet the phase requirements of the array and digitize the unit into 1-bit, the size of (l_1, l_2, l_4) can be adjusted to provide different reflection phases. The corresponding relationship between these reflection phases and the unit length is shown in Figure 9. As can be seen from Figure 9, the phase after rotation is only related to l_4, which further indicates that lower layer current does not provide the phase required for POSITION 3. This indicates that the element improvement has been successfully achieved, and the sizes of l_1, l_2, l_4 are summarized in Table 3.

TABLE 3. Expected reflection phase corresponding to different sizes.

Phase shift combination	l_1	l_2	l_4/l_5
$-90° \sim -90° \sim -90°$	8.3 mm	8.3 mm	9.50 mm
$-90° \sim -90° \sim 90°$	8.3 mm	8.3 mm	8.89 mm
$-90° \sim 90° \sim -90°$	8.3 mm	10.50 mm	9.50 mm
$-90° \sim 90° \sim 90°$	8.3 mm	10.50 mm	8.89 mm
$90° \sim -90° \sim -90°$	10.50 mm	8.3 mm	9.50 mm
$90° \sim -90° \sim 90°$	10.50 mm	8.3 mm	8.89 mm
$90° \sim 90° \sim -90°$	10.50 mm	10.50 mm	9.50 mm
$90° \sim 90° \sim 90°$	10.50 mm	10.50 mm	8.89 mm

Similarly, based on the phase distribution shown in Figures 2(d), (e), and (f), as well as the relationship between the sizes in Table 3 and the reflection phases, the PD metasurface is realized. Figure 10 shows the respective patterns of the metasurfaces that produce different focal positions. The simulation results show that under the fixed vertical polarization illumination of the metasurface, by rotating the lower layer, it is possible to switch between the two focal positions at POSITION 1 and POSITION 2, and by rotating the upper layer, it is possible to achieve focusing at POSITION 3, realizing single polarization three-focus adjustability.

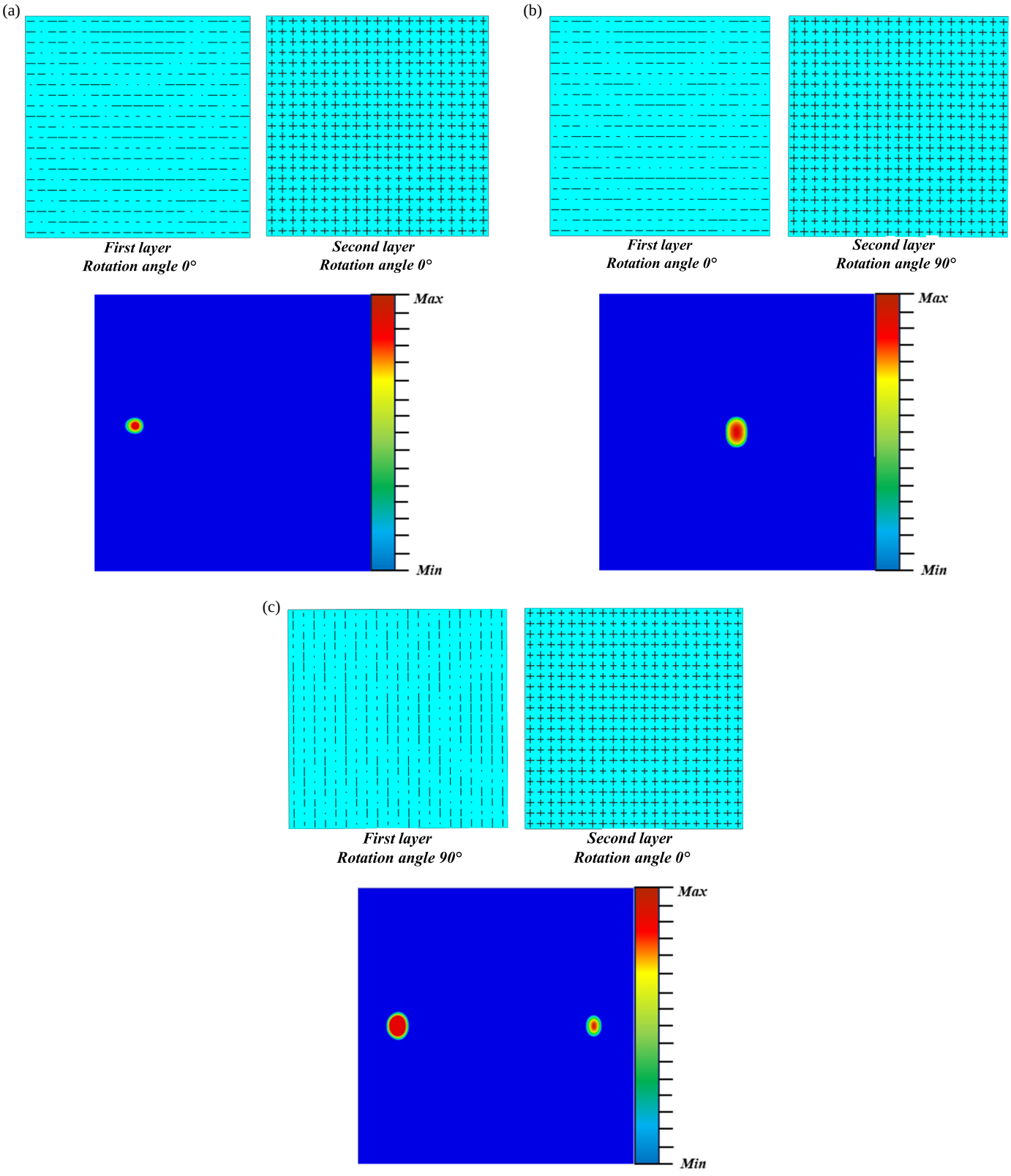

FIGURE 7. The focusing effect of the array, (a) POSITION 1; (b) POSITION 2; (c) POSITION 3.

5. TEST RESULT

The near-field focusing metasurface array with adjustable focal points was processed using planar printed circuit board technology. Due to cost constraints, the array is composed of 15×15 metasurface elements. 15 mm is reserved around the perimeter of the array for the fixation of the upper and lower layers

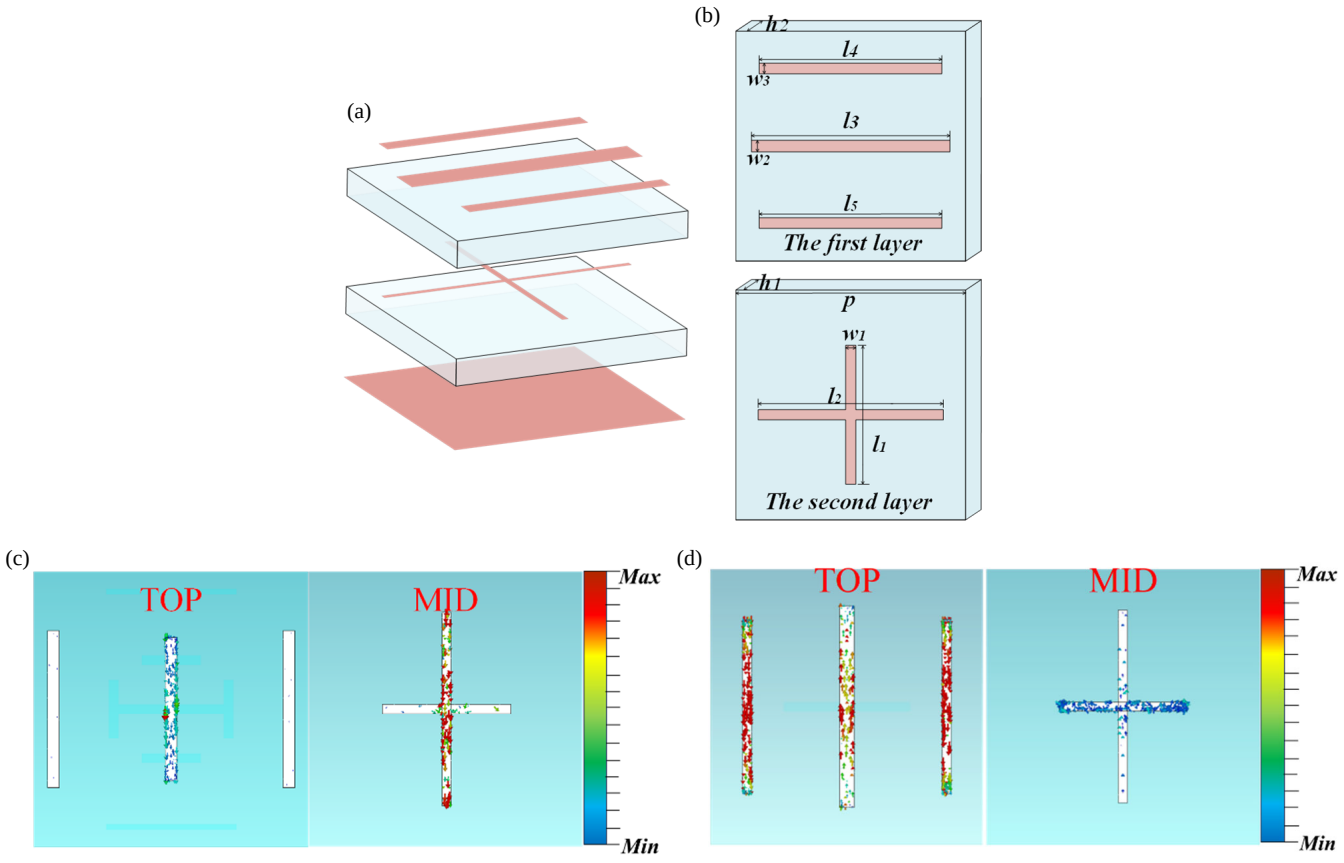

FIGURE 8. Schematic of the designed metasurface unit structure. (a) Side view; (b) top view; (c) current distribution before rotation; (d) current distribution after rotation.

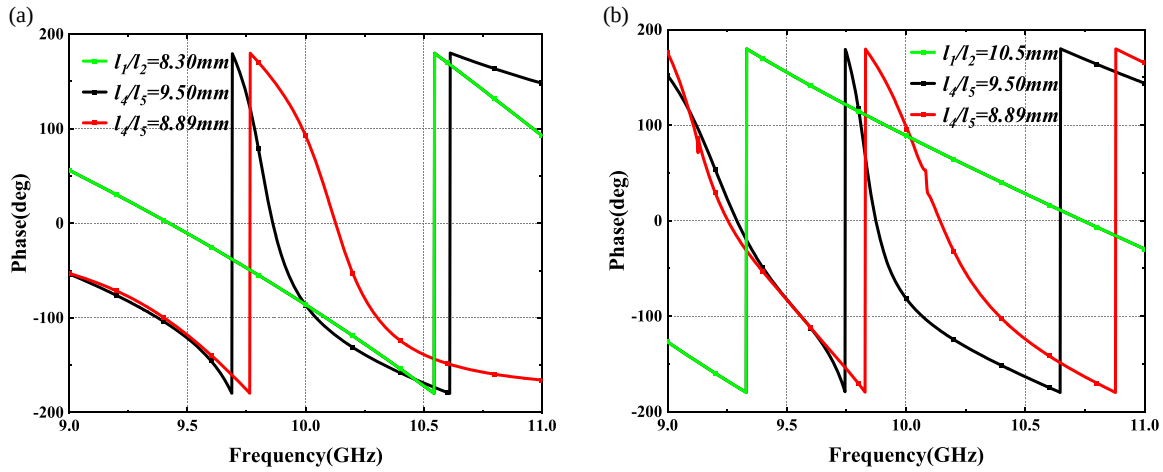

FIGURE 9. Phase characteristics.

to enable the rotation of the array. The size of the metasurface prototype is $240\,\text{mm} \times 240\,\text{mm}$. During the testing, a standard gain horn antenna operating at 10 GHz was selected as the feed source. As the array is a reflective metasurface, there may be instances during testing where the horn blocks the reflected waves. Therefore, a spherical wave oblique incidence was employed. The reflection testing system set up in a microwave anechoic chamber is shown in Figure 11(a). The sample is placed at $z = 0\,\text{mm}$, with the center of the prototype serving as the origin of the coordinate system. The probe and feed horn antenna are aligned in the same direction. The phase center of the horn antenna is located at $z = 120\,\text{mm}$, $y = -90\,\text{mm}$. Three adjustable focal points are set: POSITION 1 is located at $(-25, 90, 170)\,\text{mm}$, POSITION 2 located at $(25, 90, 170)\,\text{mm}$, and POSITION 3 located at $(0, 90, 170)\,\text{mm}$. During the testing process, the horn remains fixed, while the rotation of the meta-

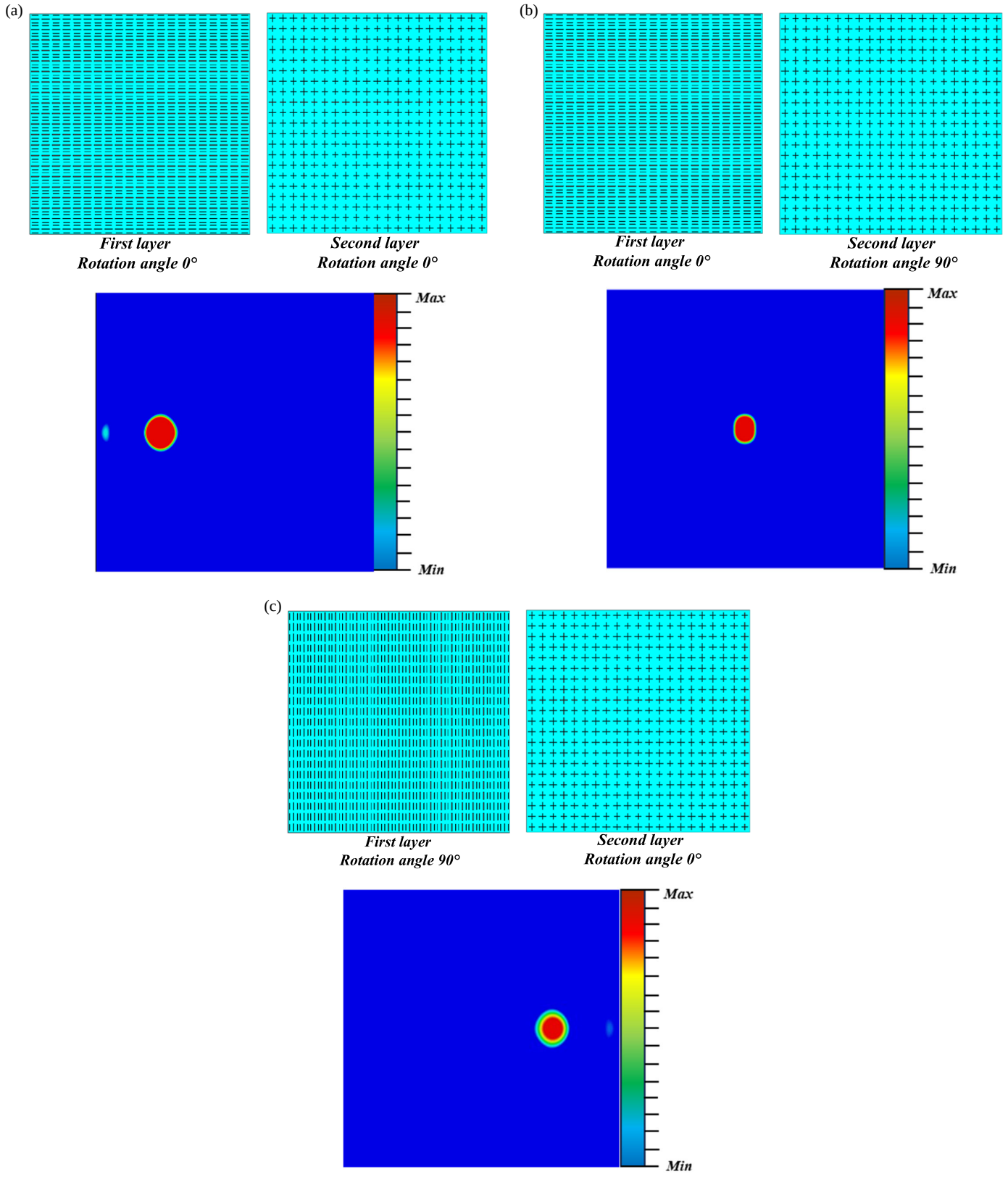

FIGURE 10. The focusing effect of the array, (a) POSITION 1; (b) POSITION 2; (c) POSITION 3.

surface array requires the upper and lower layers to be separated and manually manipulated. The probe scanned a region centered at (0, 90, 170) mm with a length of 100 mm and a width of 50 mm, using a step size of 2 mm. The three sets of actual test results obtained were processed collectively, as shown in Figure 11(b). Compared with the preset targets, the prototype

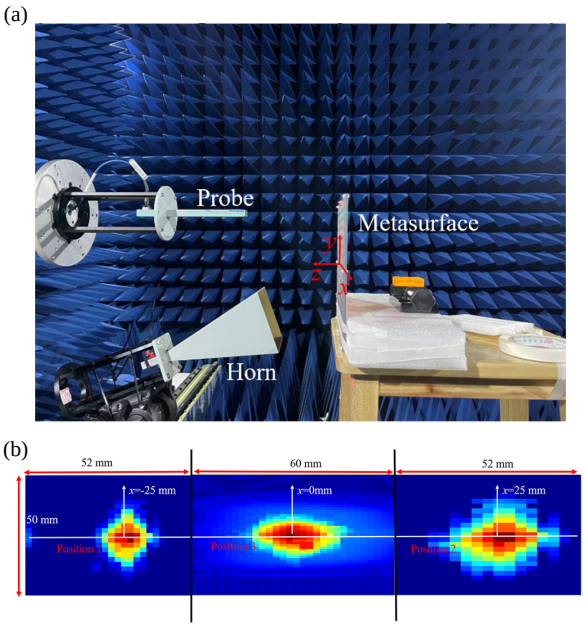

FIGURE 11. Metasurface test. (a) Test scenario; (b) Test result.

demonstrated effective focusing at the three positions, indicating the validity of achieving adjustable focal points through rotating the array.

6. CONCLUSION

In this paper, a 1-bit metasurface with adjustable three focal points under fixed polarization illumination was designed. By rotating the cross-shaped patches in the lower layer, focusing at POSITION 1 and POSITION 2 can be achieved, and by rotating the rectangular patches in the upper layer, focusing at POSITION 3 can be achieved. At the same time, by increasing the width of the upper rectangular patches and adding accompanying patches, the current of the lower cross-shaped patches is completely blocked, which solves the problem of generating focus at POSITION 1 when focusing at POSITION 3. This metasurface achieves three channels under single polarization, greatly improving the number of functions of passive metasurfaces and can be used in imaging systems, wireless power transmission and other scenarios.

ACKNOWLEDGEMENT

This work was supported by the Tian Di Science & Technology Co., Ltd Science and Technology Innovation Startup Capital Special Project (2021-TD-MS009), and Chongqing Natural Science Foundation General Program (No. CSTB2022NSCQ-MSX0960).

REFERENCES

[1] Yu, S., H. Liu, and L. Li, "Design of near-field focused metasurface for high-efficient wireless power transfer with multifocus characteristics," *IEEE Transactions on Industrial Electronics*, Vol. 66, No. 5, 3993–4002, 2019.

[2] Garnica, J., R. A. Chinga, and J. Lin, "Wireless power transmission: From far field to near field," *Proceedings of the IEEE*, Vol. 101, No. 6, 1321–1331, 2013.

[3] Lipworth, G., J. Ensworth, K. Seetharam, D. Huang, J. S. Lee, P. Schmalenberg, T. Nomura, M. S. Reynolds, D. R. Smith, and Y. Urzhumov, "Magnetic metamaterial superlens for increased range wireless power transfer," *Scientific Reports*, Vol. 4, No. 1, 3642, 2014.

[4] Li, P., M. Lewin, A. V. Kretinin, J. D. Caldwell, K. S. Novoselov, T. Taniguchi, K. Watanabe, F. Gaussmann, and T. Taubner, "Hyperbolic phonon-polaritons in boron nitride for near-field optical imaging and focusing," *Nature Communications*, Vol. 6, 7507, 2015.

[5] Ludwig, A., J. P. S. Wong, A. Epstein, A. M. H. Wong, G. V. Eleftheriades, and C. D. Sarris, "Focusing and steering for medical applications with magnetic near-field arrays and metasurfaces," in *2015 9th European Conference on Antennas and Propagation (EuCAP)*, 1–4, Lisbon, Portugal, Apr. 2015.

[6] Buffi, A., A. A. Serra, P. Nepa, H.-T. Chou, and G. Manara, "A focused planar microstrip array for 2.4 GHz RFID readers," *IEEE Transactions on Antennas and Propagation*, Vol. 58, No. 5, 1536–1544, 2010.

[7] Hansen, R., "Focal region characteristics of focused array antennas," *IEEE Transactions on Antennas and Propagation*, Vol. 33, No. 12, 1328–1337, 1985.

[8] Tofigh, F., J. Nourinia, M. N. Azarmanesh, and K. M. Khazaei, "Near-field focused array microstrip planar antenna for medical applications," *IEEE Antennas and Wireless Propagation Letters*, Vol. 13, 951–954, 2014.

[9] Karimkashi, S. and A. A. Kishk, "Focusing properties of fresnel zone plate lens antennas in the near-field region," *IEEE Transactions on Antennas and Propagation*, Vol. 59, No. 5, 1481–1487, 2011.

[10] Yu, N., P. Genevet, M. A. Kats, F. Aieta, J.-P. Tetienne, F. Capasso, and Z. Gaburro, "Light propagation with phase discontinuities: Generalized laws of reflection and refraction," *Science*, Vol. 334, No. 6054, 333–337, 2011.

[11] Zhao, M., S. Zhu, H. Huang, D. Hu, X. Chen, J. Chen, and A. Zhang, "Frequency-polarization sensitive metasurface antenna for coincidence imaging," *IEEE Antennas and Wireless Propagation Letters*, Vol. 20, No. 7, 1274–1278, 2021.

[12] Tao, M., M. Zhao, N. Zhou, and S. Zhu, "W-band frequency-polarization-diverse metasurface antenna for coincidence imaging," in *2022 PhotonIcs & Electromagnetics Research Symposium (PIERS)*, 317–323, Hangzhou, China, Apr. 2022.

[13] Ratni, B., A. d. Lustrac, G.-P. Piau, and S. N. Burokur, "Reconfigurable metasurface as microwave reflectors and polarization converters," in *2018 Asia-Pacific Microwave Conference (APMC)*, 1375–1377, Kyoto, Japan, Nov. 2018.

[14] Han, J., L. Li, S. Tian, G. Liu, H. Liu, and Y. Shi, "Millimeter-wave imaging using 1-bit programmable metasurface: Simulation model, design, and experiment," *IEEE Journal on Emerging and Selected Topics in Circuits and Systems*, Vol. 10, No. 1, 52–61, 2020.

[15] Li, W., Y. M. Wang, Y. Hei, B. Li, and X. Shi, "A compact low-profile reconfigurable metasurface antenna with polarization and pattern diversities," *IEEE Antennas and Wireless Propagation Letters*, Vol. 20, No. 7, 1170–1174, 2021.

[16] Mei, P., G. F. Pedersen, and S. Zhang, "Generation of sum and difference radiation beams with a 2-bit polarization-dependent metasurface," in *2022 16th European Conference on Antennas and Propagation (EuCAP)*, Madrid, Spain, Apr. 2022.

[17] Zhang, P., L. Li, X. Zhang, H. Liu, and Y. Shi, "Design, measurement and analysis of near-field focusing reflective metasurface for dual-polarization and multi-focus wireless power transfer," *IEEE Access*, Vol. 7, 110 387–110 399, 2019.

[18] Li, Z., Y. Zhang, H. Huang, S. Qin, K. Jie, H. Liu, J. Guo, H. Meng, F. Wang, X. Yang, and Z. Wei, "Dual-channel metasurfaces for independent and simultaneous display in near-field and far-field," *Optics Express*, Vol. 30, No. 11, 18 434–18 446, 2022.

[19] Li, J., Y. Yuan, Q. Wu, S. N. Burokur, and K. Zhang, "Dual-band independent phase control based on high efficiency metasurface," *Chinese Optics Letters*, Vol. 19, No. 10, 100501, 2021.

[20] Liu, W., Y. Zhuo, L. Xiao, C. Chen, S. Shang, H. Liu, H. Meng, F. Wang, X. Yang, and Z. Wei, "Four-channel metasurface for multiplexing images under two nonorthogonal polarization states," *Chinese Optics Letters*, Vol. 21, No. 9, 093601, 2023.